Environ Fluid Mech (2006) 6:573–592
DOI 10.1007/s10652-006-9007-2

ORIGINAL ARTICLE

Structure of turbulent plumes from a momentumless source in a smooth bed

J. P. Crimaldi · J. R. Koseff

Received: 17 July 2006 / Accepted: 7 September 2006 /
Published online: 7 October 2006

Abstract The spatial development of a passive scalar plume is studied within the inhomogeneous turbulence of a boundary layer flow in a recirculating laboratory flume with a smooth bed. The source of the scalar is located flush with the bed, and the low-momentum source design is intended to simulate a diffusive-type scalar release. A weakly diffusive fluorescent dye is used as the scalar. Planar laser-induced fluorescence (PLIF) techniques were used to record the structure of the plume at a spatial resolution of 150 μm. The measured structure of the mean concentration field is compared to an analytical solution for shear-free, homogeneous turbulence. The laboratory plume exhibits spatial development in the mean concentration field that deviates from the self-similar behavior predicted by the analytical solution; this deviation is due to the mean shear and inhomogeneity of the turbulence. In particular, the influence of the viscous sublayer on the plume development is seen to be significant. Nonetheless, the analytical solution replicates some of the features seen in the laboratory plume, and the solution suggests methods of reducing the laboratory data even for cases where the results deviate from the analysis. We also examine the spatial development of the root-mean-square (rms) fluctuating concentration field, and use scalar probability density functions to examine the relationship between the mean and fluctuating concentrations.

Keywords Boundary layer · Scalar structure · Turbulent plumes

J. P. Crimaldi (✉)
Department of Civil, Environmental, and Architectural Engineering, University of Colorado, Boulder, CO 80304-0428, USA e-mail: crimaldi@colorado.edu

J. R. Koseff
Department of Civil and Environmental Engineering Stanford University, Stanford, CA 94305-4020, USA

1 Introduction

The macroscopic dispersion of passive scalars from momentumless sources is governed exclusively by details of the mean and instantaneous flow structure. Within a turbulent boundary layer, the process is complicated by the anisotropic and inhomogeneous nature of the turbulence. In this study, we examine the spatial development of a neutrally buoyant passive scalar dye plume introduced with extremely low momentum from a flush source in the smooth bed of a laboratory water flume. The source configuration was designed to mimic a diffusive-type scalar release from within a smooth bed; the interaction of such a plume with the viscous sublayer (VSL) region of the boundary layer is seen to be significant. The plume structure is quantified in vertical and horizontal planes for two flow cases using a planar laser-induced fluorescence (PLIF) technique (1). We compare the results to an idealized analytical plume solution and to previous studies.

Laboratory flumes have been used previously to measure the plume structure from an isokinetic ground level release from a horizontal tube over a rough bed (2), from an isokinetic release in the logarithmic region of a turbulent boundary layer above smooth (3,4) and rough beds (5). The dispersion of ground level and elevated scalar releases has also been studied in wind tunnels over a rough bed (6,7). A summary of the findings from these studies is given in Rahman and Webster (5).

The effect of inhomogeneity in the turbulent boundary layer on plume dispersion has been investigated analytically (6,8) and numerically (9). Vertical variations in turbulent mixing result in a non-Gaussian vertical concentration profile, but lateral concentration profiles remain Gaussian. Several studies (2,6,7) suggest that the non-Gaussian vertical profiles are nonetheless self-similar in the streamwise direction. The results of this study indicate a strong streamwise development in the shape of the vertical profile. We argue that this is a result of a strong influence by the VSL that was absent in other experimental configurations.

Portions of the dataset presented in the present paper have been published in an earlier work by Crimaldi et al. (10). The earlier work examined the relationship between the instantaneous and mean scalar structure for a single flow case. The present study examines the spatial development of both the mean and fluctuating concentration fields for two flow cases. The results share some common features seen in previous studies, but also differ significantly in a number of important respects. In particular, the streamwise development of vertical profiles of the mean concentration shows a *decrease* in kurtosis, asymptoting toward a Gaussian in the far field. Previous studies (over rough boundaries) show the opposite trend.

2 Ideal plume solution

We begin by reviewing the analytical framework for an idealized scalar plume, ignoring mean shear and inhomogeneous diffusivities in the flow. The resulting solution will be useful as a baseline for the experimental results presented later. The steady-state turbulent transport of a passive scalar in a flowfield with mean velocity $(\overline{u}, 0, 0)$ is given by

$$\overline{u}\frac{\partial \overline{C}}{\partial x} = \frac{\partial}{\partial y}\left(D_y \frac{\partial \overline{C}}{\partial y}\right) + \frac{\partial}{\partial z}\left(D_z \frac{\partial \overline{C}}{\partial z}\right), \tag{1}$$

where $\overline{C}$ is the local mean concentration, and D_y and D_z are effective diffusivities due to turbulent dispersion in the lateral and vertical directions (streamwise diffusion is negligible relative to the advective scalar flux). Equation 1 has simple analytical solutions when neither the velocity field nor the turbulent diffusivities vary spatially. For an ideal flow in the x-direction over a solid boundary located at $z = 0$, with a point scalar source located at $(0, 0, 0)$ continuously releasing scalar mass at rate $\dot{m}$, the solution to Eq. 1 is a plume given by

$$\overline{C}(x, y, z) = \frac{2\dot{m}}{4\pi x\sqrt{D_y D_z}} \exp\left(-\frac{y^2}{2\sigma_y^2} - \frac{z^2}{2\sigma_z^2}\right), \tag{2}$$

where lateral and vertical concentration profiles are Gaussian with standard deviations

$$\sigma_y = \sqrt{2D_y x/\overline{u}} \tag{3}$$

and

$$\sigma_z = \sqrt{2D_z x/\overline{u}}\,. \tag{4}$$

Both lateral and vertical mean concentration profiles are self-similar, with plume dimensions that grow as $x^{1/2}$ and magnitudes that decay as x^{-1}. This ideal plume solution will be used as a baseline for comparing the development of a plume in a real turbulent boundary layer (where velocities and coefficients of turbulent dispersion vary spatially). This will enable us to investigate the effect of inhomogeneous turbulence and mean shear on the spatial development of the plume.

3 Experimental details

Plume image data were collected in an open-channel recirculating flume (Fig. 1). A turbulent boundary layer is tripped by a 3 mm diameter rod that spans the flume at the upstream end of the flume. The boundary layer then develops over a smooth bed of Plexiglas. The plume source location, designated $(x, y, z) = (0, 0, 0)$, is on the

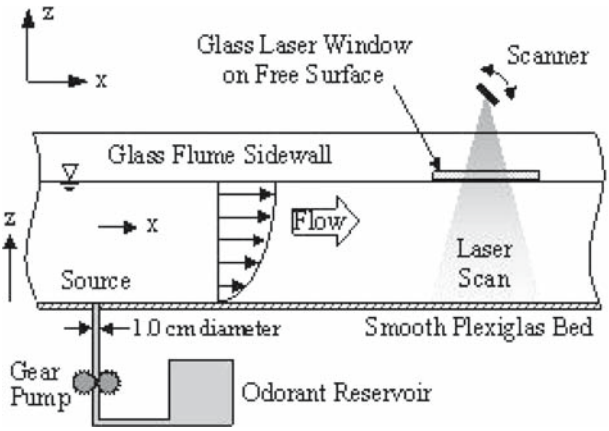

Fig. 1 Side view of the flume test section showing the plume source location and coordinate system (vertical laser scan configuration shown)

Table 1 Summary of the two experimental flow conditions used in this study

U_∞ (cm/s)	u_τ (cm/s)	δ(cm)	Re_θ
9.84	0.488	7.2	540
29.9	1.28	7.0	1,800

The values shown were measured at $x = 160$ cm

centerline of the flume bed, 2.2 m downstream of the trip rod, and the test section continues 3 m downstream from the source. The source is designed to mimic a diffusive-type (i.e., momentumless) release of a scalar from a flush, bed-level location. A 20 ppm aqueous solution of the fluorescent dye Rhodamine 6G (Schmidt number = 1,250 (11)) is used for the scalar. A gear pump is used to pump the dye solution slowly through a 1 cm diameter circular hole drilled in the floor of the flume. The hole is filled with a porous foam to provide a uniform flow across the source exit; the foam is mounted flush with the bed of the flume. The dye solution is pumped at a volumetric rate of 3 ml/ min, resulting in a vertical exit velocity of 0.063 cm/s. Further details of the flume design can be found in Crimaldi et al. (10).

Results are presented for two flow cases, with freestream velocities of approximately $U_\infty = 10$ and 30 cm/s. A two-dimensional laser-Doppler velocimeter (LDV) was used to record vertical profiles of the mean velocities and turbulence structure at $x = 160$ cm for both flow cases. Pertinent parameters for each flow case are summarized in Table 1. The shear velocities u_τ were calculated by fitting the mean velocity profiles to the "law of the wall" (see Fig. 2b). The boundary layer depth δ was estimated as the location where $U = 0.99U_\infty$.

Vertical profiles of the mean streamwise (U) and vertical (W) velocities are shown dimensionally in Fig. 2a. Non-dimensional streamwise velocities are shown in Fig. 2b,

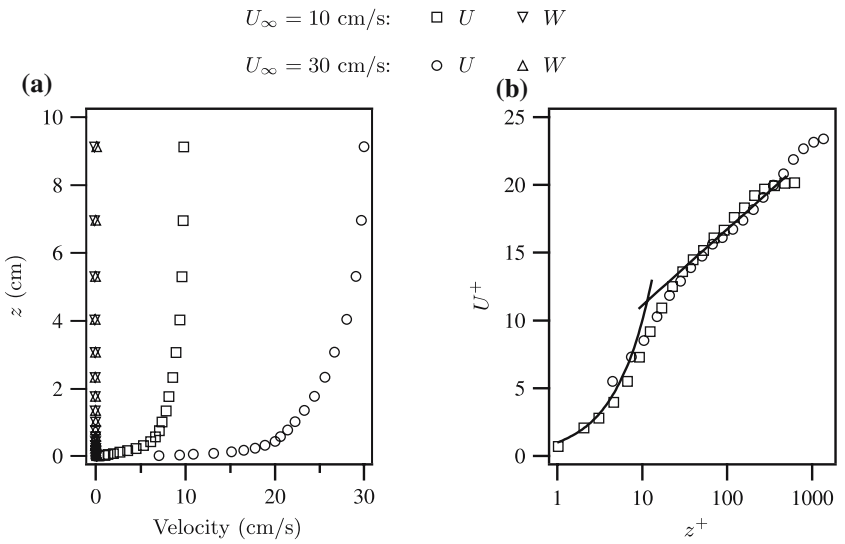

Fig. 2 Mean streamwise (U) and vertical (W) velocity profiles for the two flow cases used in this study. The profiles were measured at $x = 160$ cm using an LDV. **(a)** Dimensional profiles of U and W. **(b)** Streamwise velocity profiles plotted as U^+ versus z^+

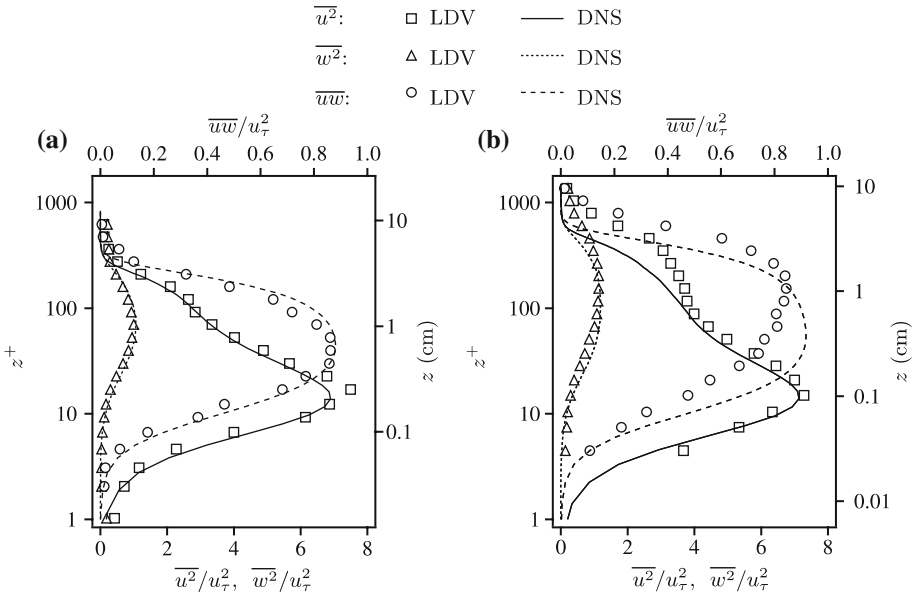

Fig. 3 Turbulence intensity and Reynolds stress data (*symbols*) measured at $x = 160$ cm for **(a)** $U_\infty = 10$ cm/s and **(b)** $U_\infty = 30$ cm/s . For comparison, DNS results (*lines*) by Spalart at **(a)** $\mathrm{Re}_\theta = 670$ and **(b)** $\mathrm{Re}_\theta = 1,410$ are shown

where the solid lines are the analytical expressions $U^+ = z^+$ and $U^+ = (1/\kappa)\ln z^+ + 5.5$, where $U^+ = U/u_\tau$ and $z^+ = zu_\tau/\nu$.

Figure 3 contains measured vertical profiles of normalized turbulence statistics, with the $U_\infty = 10$ cm/s data shown in Fig. 3a and the $U_\infty = 30$ cm/s data shown in Fig. 3b. In each case, the data are compared with direct numerical simulation (DNS) results by Spalart (12) at Reynolds numbers that are similar to the laboratory conditions.

Streamwise and vertical turbulence intensities $\overline{u^2}$ and $\overline{w^2}$, and the Reynolds stress correlation $\overline{uw}$ are normalized by u_τ^2, the square of the shear velocity. The statistics are plotted versus both the non-dimensional wall distance z^+ as well as the dimensional distance z. These data are useful for understanding the hydrodynamic context of the plume results presented later.

Digital images of instantaneous plume concentrations were obtained using a PLIF technique. Details of the imaging apparatus, image acquisition, and image processing are given by Crimaldi and Koseff (1) and Crimaldi et al. (10). Images were acquired at various locations in both horizontal and vertical planes aligned parallel to the flow. At a given location for a given flow case, 8,000 images were typically acquired at a frame rate of 3 Hz. The individual images of instantaneous concentration fields were then ensemble averaged to produce images of statistics such as mean and root-mean-square (rms) concentrations. Sample images of instantaneous, mean, and rms concentrations are shown for a horizontal plane in Fig. 4 and a vertical plane in Fig. 5. Both figures correspond to data acquired in the vicinity of $x = 100$ cm for the $U_\infty = 10$ cm/s flow case.

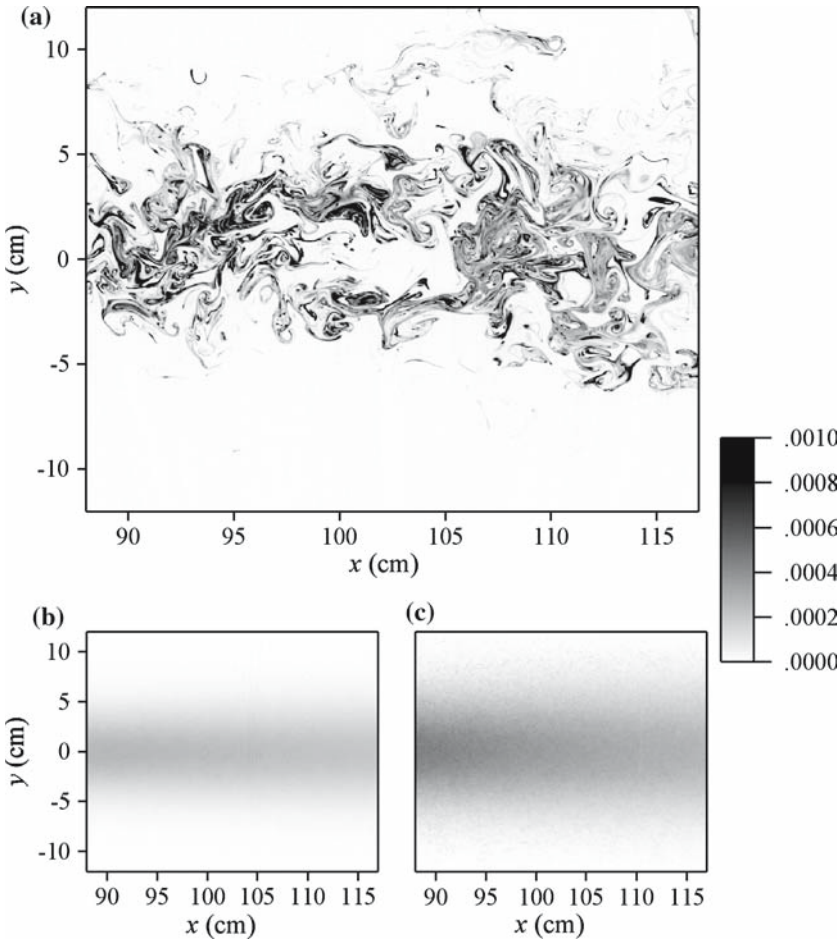

Fig. 4 Sample PLIF image data in a horizontal plane at $z = 2$ cm. **(a)** Typical instantaneous concentration, **(b)** Mean concentration, and **(c)** rms concentration. All values are normalized by the source concentration, and plotted using the grayscale shown in the legend

4 Results

4.1 Spatial development of the mean concentration field

We begin by examining the spatial development of the mean concentration field, using image data acquired as described in the previous section. In particular, we compare the measured spatial development with what is predicted by the ideal plume theory presented in Sect. 2

4.1.1 Lateral structure

For the ideal plume given by Eq. 2, the lateral structure of the mean concentration field consists of Gaussian profiles with a maximum concentration on the plume centerline.

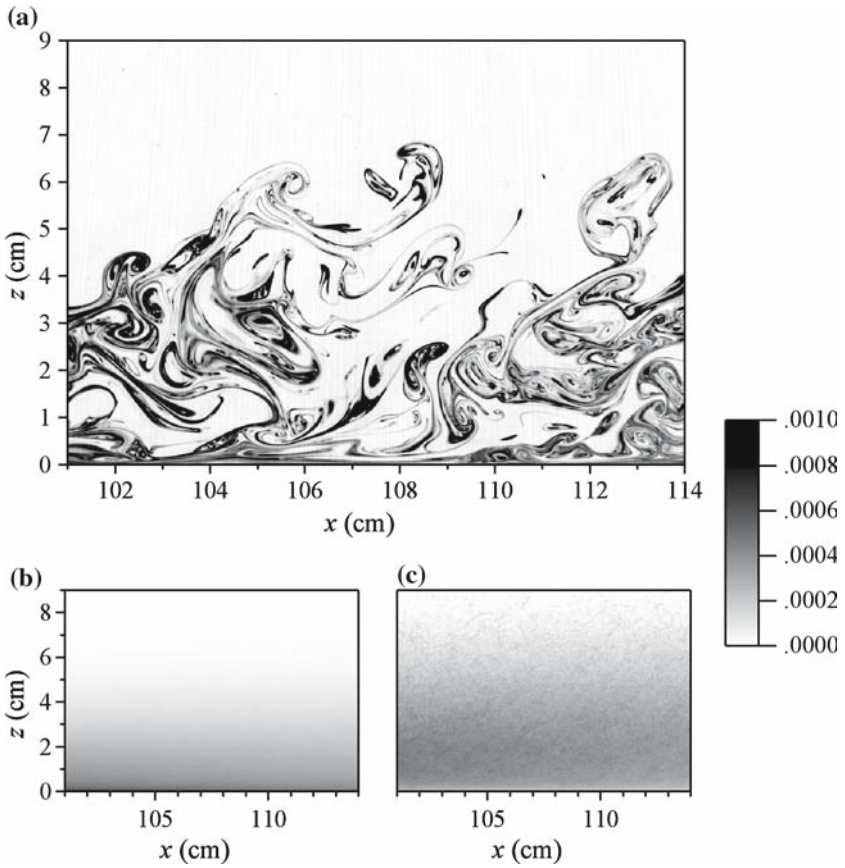

Fig. 5 Sample PLIF image data in a vertical plane at $y = 0$ cm. **(a)** Typical instantaneous concentration, **(b)** Mean concentration, and **(c)** rms concentration. All values are normalized by the source concentration, and plotted using the grayscale shown in the legend

These profiles can be expressed in the self-similar form

$$\frac{\overline{C}(y)}{\overline{C}_{y=0}} = \exp\left(\frac{-y^2}{2\sigma_y^2}\right), \tag{5}$$

where $\overline{C}_{y=0}$ is the mean centerline concentration of a given plume profile, and σ_y is a measure of the plume width (Eq. 3). Lateral profiles of mean concentration normalized in this manner are shown in Fig. 6, where a two-parameter least-squares fit is performed for each profile to obtain values for $\overline{C}_{y=0}$ and σ_y. Data (symbols) from both flow cases and for various x and z locations are compared with Eq. 5 (solid line). The mean lateral concentration profiles are Gaussian, consistent with the ideal plume theory and previous experimental studies (2,7).

The streamwise growth of σ_y as a function of streamwise location is shown in Figs. 7 and 8 for both flow cases and at several heights above the bed. The dimensional data are compared to the growth given by the ideal plume solution in Eq. 3.

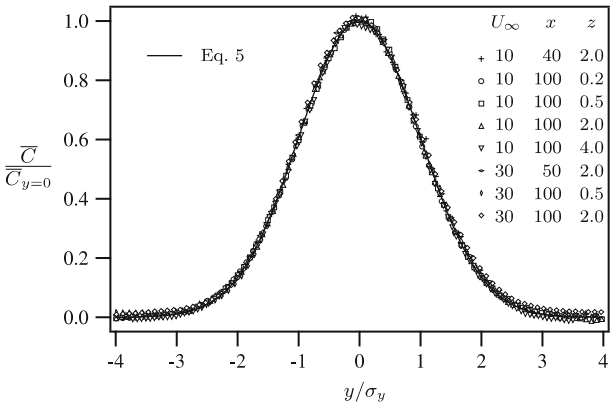

Fig. 6 Normalized lateral profiles of mean concentration, with only every tenth data point shown for clarity. *Units* in the legend are in terms of cm/s for U_∞ and cm for x and z. The *solid line* underneath the symbols is the Gaussian given by Eq. 5

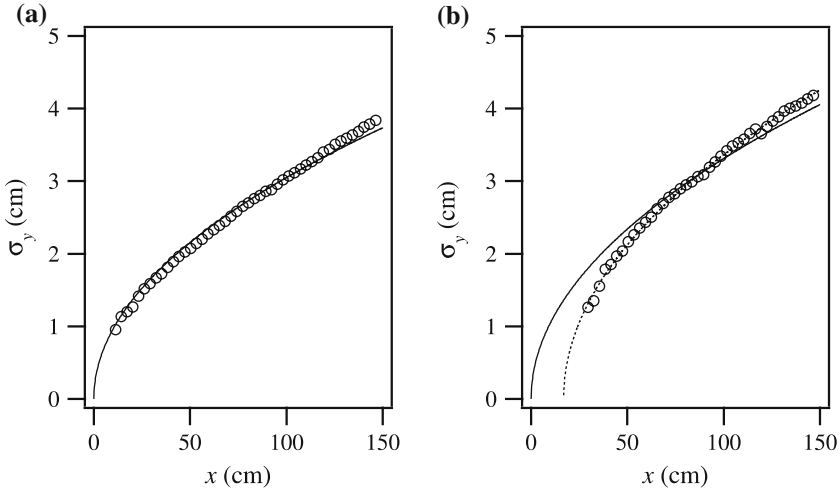

Fig. 7 Lateral plume growth at **(a)** $z = 2$ cm and **(b)** $z = 4$ cm as a function of downstream distance from the source for $U_\infty = 10$ cm/s. The *solid lines* are fits of Eq. 3 to the data. The *dashed line* is a similar fit, but including an x-offset as an additional fit parameter

In Fig. 7, data (symbols) are shown for the $U_\infty = 10$ cm/s flow case at (a) $z = 2$ cm and (b) $z = 4$ cm above the bed. For each case, a least-squares fit of Eq. 3 (solid line) is shown, where the fit parameter allows D_y to be calculated (by assuming $\overline{u} = U_\infty$ in Eq. 3). At $z = 2$ cm, the data are in excellent agreement with the ideal plume solution. Farther from the bed, at $z = 4$ cm, the fit is not quite as good. However, if a new fit is performed where an x offset is introduced as a second fitting parameter, the agreement is improved. This fit is shown in Fig. 7b as a dotted line. This finding suggests that the combined effects of shear and vertical variations in mixing rates results in a downstream shift in the effective origin for the $x^{1/2}$ growth of σ_y. This effect appears to be larger at distances farther from the wall.

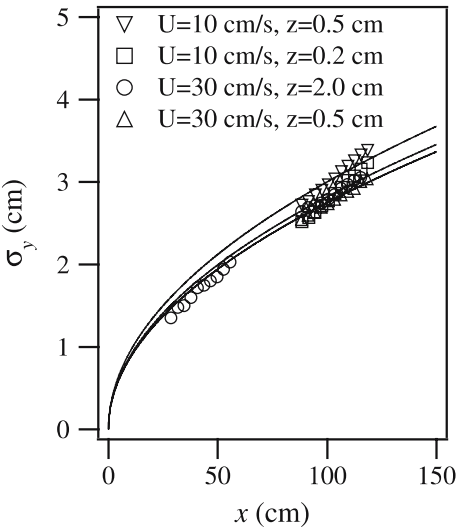

Fig. 8 Additional lateral plume growth data (*symbols*) compared with fits of Eq. 3 (*solid lines*)

Table 2 Lateral diffusivities

U_∞	z (cm)	D_y (cm^2/s)	$D_y/(\delta u_\tau)$
10	4	0.54	0.15
10	2	0.46	0.13
10	0.5	0.44	0.13
10	0.2	0.39	0.11
30	2	1.13	0.13
30	0.5	1.13	0.13

Additional σ_y versus x data are shown in Fig. 8. For the cases shown in this plot, we had acquired images over a much shorter range of x values, but fits to estimate D_y were still possible. The resulting D_y values for all of the cases are summarized in Table 2. Note that, for simplicity, all tabulated data represents values of D_y obtained without the use of an x-offset fitting parameter.

Also tabulated are values of $D_y/(\delta u_\tau)$, where δ is the depth of the momentum boundary layer in the vicinity of the developing plume. Empirical values of the parameter $D_y/(d\, u_\tau)$, where d is the flow depth, are commonly reported in range from 0.1 to 0.2, with a typical empirical estimate being $D_y \approx 0.15 d u_\tau$ (13). In our laboratory study, the momentum boundary layer is not fully developed over the depth of the flow, so the use of the boundary layer depth δ is a more consistent parameter than d. The measured values of $D_y/(\delta u_\tau)$ are in all cases in reasonable agreement with published empirical estimates. However, the near-bed values are smaller by as much as 25%, consistent with the idea of lower lateral mixing rates near the bed.

4.1.2 Vertical structure

For the ideal plume solution, the vertical structure of the mean concentration field also consists of Gaussian profiles, with a maximum concentration at the bed. Using Eq. 2, vertical concentration profiles along the ideal plume centerline ($y = 0$) can be

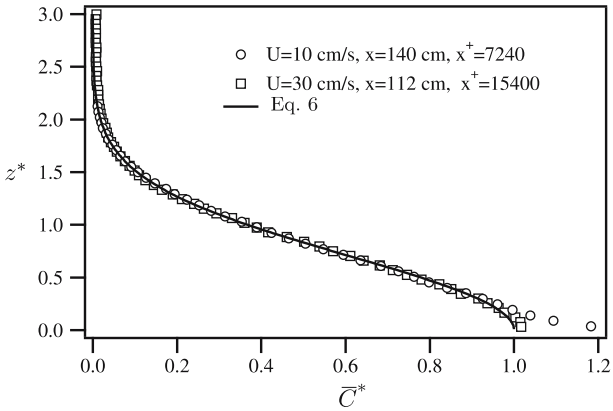

Fig. 9 Vertical profiles of mean concentration at downstream locations for both flow cases, plotted in the non-dimensional form given by Eq. 7. The *line* is the ideal plume solution given by Eq. 6

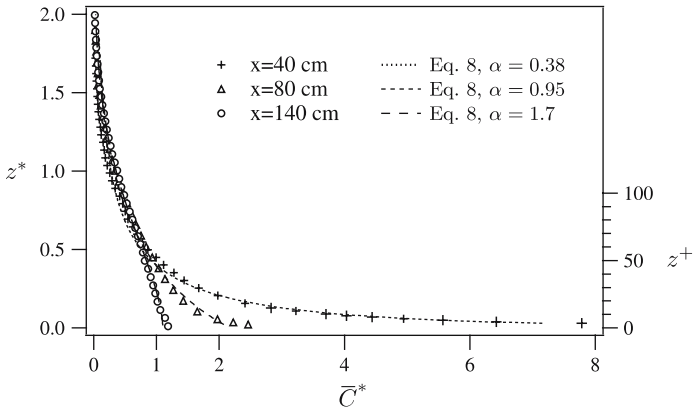

Fig. 10 Vertical profiles of mean concentration at various streamwise locations for the $U_\infty = 10\,\mathrm{cm/s}$ flow case, plotted in the same non-dimensional form as Fig. 9 (note that the vertical locations are also given in terms of z^+ units on the right-hand axis). The *dashed lines* are least-squares fits of the three profiles to Eq. 8, with resulting α vales as shown

written in the self-similar form

$$\overline{C}^* = \exp\left(-z^{*2}\right), \tag{6}$$

where

$$\overline{C}^* = \frac{2\pi\sqrt{D_y D_z}}{\dot{m}} xC \qquad \text{and } z^* = \sqrt{\frac{\overline{u}}{4D_z}}\frac{z}{\sqrt{x}}. \tag{7}$$

Measured vertical concentration profiles far from the source are quite consistent with Eq. 6. Figure 9 shows downstream vertical profiles from each of the two flow cases. Each of the profiles is normalized via a least-squares fit to Eq. 6. The fit yields values for the parameters $2\pi\sqrt{D_y D_z}/\dot{m}$ and $\sqrt{\overline{u}/4D_z}$ in Eq. 7. Since neither of these parameters are expected to vary significantly in the x direction, the same values are then used later to non-dimensionalize the remaining vertical profiles closer to the source.

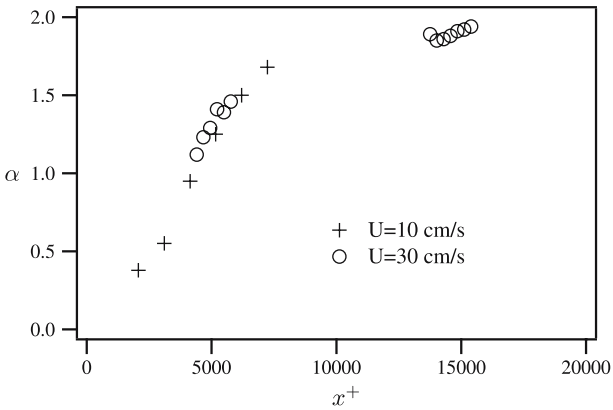

Fig. 11 Values of α obtained via least-squares fits of vertical concentration profiles to Eq. 8 for both flow cases. The distances from the source are normalized by the viscous length scale such that $x^+ = xu_\tau/\nu$

Near the bed, the measured concentrations exceed the ideal predictions. This effect is greater for the slower flow case, and becomes more pronounced for both flow cases closer to the source. The distance from the source is normalized by the viscous length scale, giving $x^+ = xu_\tau/\nu$.

Figure 10 shows the streamwise development of the vertical concentration profiles for the $U_\infty = 10$ cm/s flow case. All three profiles are normalized by the same values used for the $x = 140$ cm data in Fig. 9. Close to the source, the near-bed concentration values greatly exceed the ideal prediction (see the solid line from Fig. 9), consistent with observed "trapping" of dye within the low-mixing region of the VSL (10), and with corresponding lower concentrations far from the bed. The right-hand axis on Fig. 10 gives distance from the bed in terms of z^+ units. Note that the deviations above the theory grow large for $z^+ < 30$, which corresponds to the viscous wall region, and the deviations are largest in the VSL ($z^+ < 5$). Scalars in the region below $z^+ \approx 10$ are limited in their vertical motion due to the fact that the vertical turbulence intensities remain close to zero up to this distance from the bed (see Fig. 3). As distance from the source increases, the "trapped" dye eventually migrates into the overlaying flow where turbulent dispersion produces a vertical profile that approaches the ideal solution. A least-squares curve fit of the form

$$\overline{C}^* = A \exp\left(-z^{*\alpha}\right) \tag{8}$$

is also shown for each of the profiles. For the three profiles shown, the values found for the exponent α are 0.38, 0.95, and 1.7. The shape of the profiles asymptotes toward a Gaussian ($\alpha = 2$) as x increases. This trend is shown for both flow cases in Fig. 11. The data from the two flow cases compare well if the streamwise distance is normalized by the viscous length scale as x^+.

Because of the non-Gaussian nature of the vertical concentration profiles (at least near the source), the vertical spreading of the mean concentration field cannot be properly characterized in terms of the Gaussian standard deviation given by Eq. 4. We therefore define the height of the mean plume (δ_{02}) as the vertical location where the mean concentration drops to 2% of the local bed concentration (the finite spatial resolution of the camera combined with laser reflections very close to the bed forced

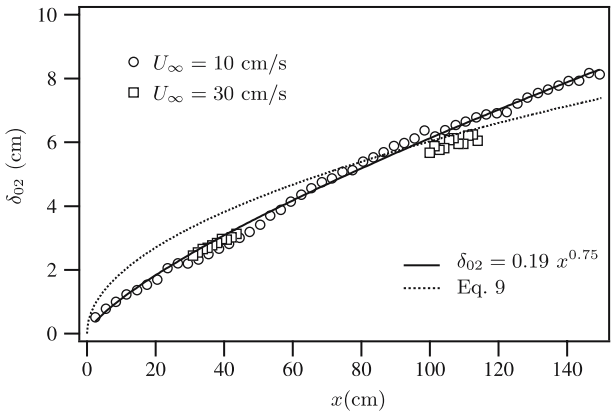

Fig. 12 Vertical plume height δ_{02} as a function of downstream distance from the plume origin for $U_\infty = 10$ cm/s and $U_\infty = 30$ cm/s. The *solid line* is a least-squares fit of $\delta_{02} = A\ x^{0.75}$ to the $U_\infty = 10$ cm/s data, and the *dotted line* is Eq. 9

us to use the measured concentration at $z = 1$ mm as the bed concentration). Figure 12 shows streamwise growth of δ_{02} for both the $U_\infty = 10$ cm/s and $U_\infty = 30$ cm/s flow cases.

From Eq. 2, the predicted growth of δ_{02} for the homogeneous turbulence plume can be calculated as

$$\delta_{02} = \sqrt{\frac{4D_z \ln 0.02}{\overline{u}}}\ x^{1/2}. \tag{9}$$

This prediction is shown as a dotted line in Fig. 12, where the value of the leading coefficient has been determined using a least-squares fit to the $U_\infty = 10$ cm/s data. It is clear that the vertical dimension of the real plume does not grow as $x^{1/2}$. The solid line has the form $\delta_{02} = A\ x^{0.75}$, consistent with the vertical growth seen by Fackrell and Robins (7) and others. Also shown in the figure are results from the $U_\infty = 30$ cm/s flow case; the δ_{02} values from these data behave similarly to the $U_\infty = 10$ cm/s data.

4.1.3 Streamwise behavior

Using Eq. 2, the streamwise mean concentration distribution along the plume centerline ($y = 0$) can be written in the self-similar form

$$z^2\ \overline{C}(x, 0, z) = \frac{2\dot{m}}{4\pi\sqrt{D_y D_z}}\ \xi^{-1} \exp -\frac{\xi^{-1}}{4D_y/\overline{u}}, \tag{10}$$

where $\xi = xz^{-2}$. Equation 10 demonstrates that the ideal $\overline{C}$ decays as x^{-1}. Motivated by this form of the ideal solution, we plot profiles of $z^2\overline{C}$ (normalized by the source strength C_0) verus the similarity variable ξ to see how the streamwise development of a plume within an inhomogeneous turbulent boundary layer compares with the self-similar profile of the ideal plume theory.

The results, shown in Fig. 13 demonstrate two points. First, the streamwise concentration profiles are not self-similar at different heights. Second, the far-field streamwise

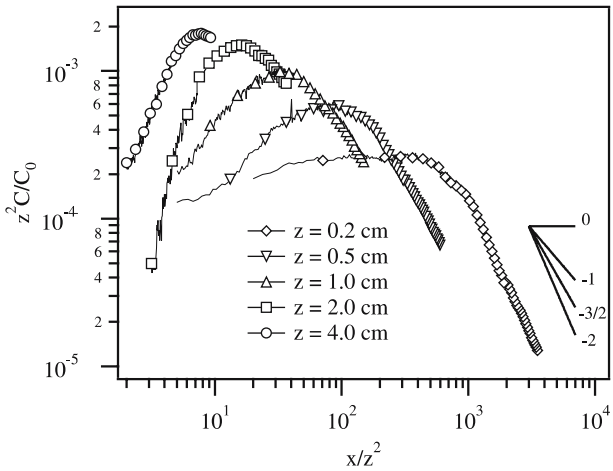

Fig. 13 Normalized streamwise evolution of mean concentration at various vertical locations for $U_\infty = 10$ cm/s

concentration decay exceeds the x^{-1} rate predicted by Eq. 10. As seen in the figure, the decay rate approaches x^{-2} for the near-bed data.

4.2 Spatial development of the fluctuating concentration field

We now continue by examining the spatial development of the fluctuating concentration field. For convenience, we use c' to denote the rms of the fluctuating component of the concentration field.

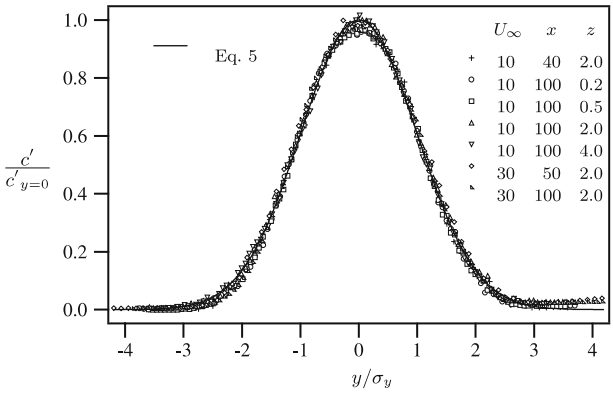

Fig. 14 Normalized lateral profiles of rms concentration fluctuation strength, with only every tenth data point shown for clarity. Units in the legend are in terms of cm/s for U_∞ and cm for x and z. The *solid line* is a Gaussian of the same form as Eq. 5

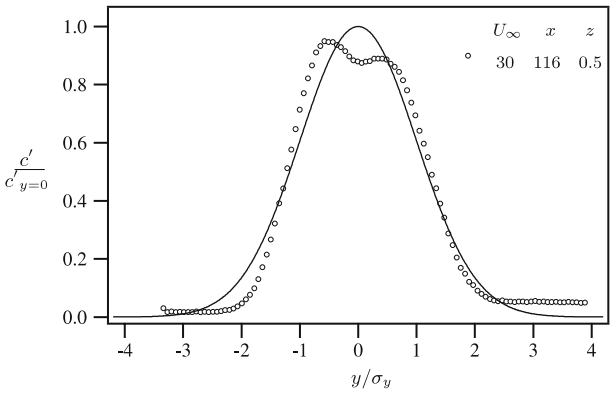

Fig. 15 Normalized lateral profiles of rms concentration fluctuation strength at $x = 116$ cm for the $U_\infty = 30$ cm/s case at $z = 0.5$ cm. *Units* in the legend are in terms of cm. The *solid line* is the Gaussian $C/\overline{C}_{y=0} = \exp(-y^2/2\sigma_y^2)$

4.2.1 Lateral behavior

Lateral profiles of c' at several streamwise and vertical locations for both flow cases are shown in Fig. 14.

The values for $c'_{y=0}$ and σ_y were obtained by fitting $c'/c'_{y=0}$ to an equation with the same form as Eq. 5, which is shown in the figure as a solid line. The lateral profiles of c' shown in the figure are Gaussian. However, the lateral c' profile from one experimental condition is not included in Fig. 14, since the behavior was quite different. This c' profile, located far from the source ($x = 116$ cm) and close to the bed ($z = 0.5$ cm) for the $U_\infty = 30$ cm/s flow case is shown in Fig. 15 (where Eq. 5 is again included for reference).

For this condition, off-axis bipolar maxima are seen in the c' profile, consistent with what has been reported in several previous studies of similar (but not identical) flows (2,7). The off-axis maxima persist over the entire streamwise range of the image data for this dataset (88 cm $\leq x \leq$ 118 cm), and the bipolar nature of the profiles grows stronger towards the downstream edge. A meandering plume model (2) suggests that off-axis maxima occur when the plume spreading is dominated by small-scale turbulent mixing rather than by mixing due to larger-scale meandering. Since the meandering scale becomes small relative to the plume width far from the source, this model predicts that off-axis maxima will occur at sufficiently large downstream distances. This distance should be reached first when turbulence levels are high (e.g., at higher velocities and close to the bed). Thus, the appearance of off-axis maxima only at $z = 0.5$ cm for $U_\infty = 30$ cm/s is consistent with this model.

We now quantify the ratio of the width of the concentration variance profiles relative to the width of the $\overline{C}$ profiles, whose growth was quantified earlier. Note that the width of the concentration variance plume is equal to the width of the c' plume divided by $\sqrt{2}$. The streamwise development of this width ratio is shown in Fig. 16 where, for simplicity, we consider only the Gaussian profiles from Fig. 14.

The ratios are near unity, with no apparent streamwise dependence. Thus, the lateral growth of the variance plume mimics that of the mean plume. As seen in the

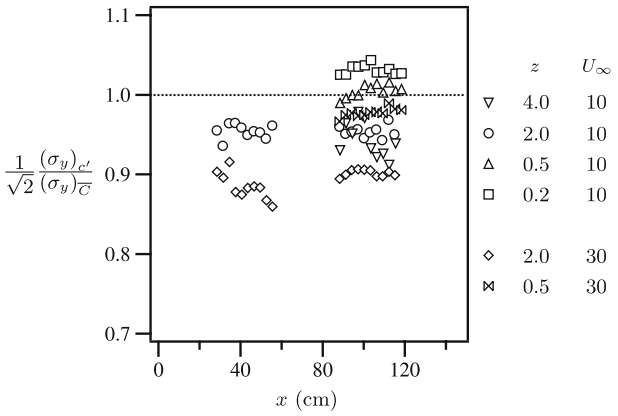

Fig. 16 Ratio of the width of the concentration variance plume to the width of the mean concentration plume (where the variance plume width is equal to the rms plume width divided by $\sqrt{2}$). In the legend, z is the distance from the bed in cm, and U_∞ is the freestream velocity in cm/s

figure, the ratio of variance width to mean concentration width generally decreases slightly as distance from the bed increases or as the velocity increases.

4.2.2 Vertical behavior

Vertical profiles of c' for the $U_\infty = 10$ cm/s flow case are shown in Fig. 17.

The two upstream profiles ($x = 32$ and 42 cm, Fig. 17a) have their maxima close to the bed level with a near-exponential decay above that. Further downstream (at $x = 102$ and 112 cm, Fig. 17b), the c' maxima is much farther above the bed. An analogous pair of plots at the same locations for the $U_\infty = 30$ cm/s flow case is shown in Fig. 18. In the upstream location (Fig. 18a), the c' peak is smaller and markedly farther from the bed as compared to the $U_\infty = 10$ cm/s flow case, due to increased scalar mixing and dissipation at the higher flowrates. Farther downstream (Fig. 18b), the magnitude and location of the c' peak are quite similar to the those for the slower flow.

For both flow cases, the c' peak is always above the bed, despite the fact that the $\overline{C}$ peak is always at the bed (compare with Fig. 10). Thus, the near-bed plume structure consists of high-mean concentrations (enhanced by scalar "trapping" in the VSL) with low-concentration fluctuations (due to rapid mixing by the high shear in the VSL, and high-turbulence intensities above the VSL).

4.3 Scalar probability density functions

Scalar probability density functions (pdf's) are useful for examining the relationship between the mean concentration and the range of instantaneous concentrations that contribute to the mean. We calculated pdf's of scalar concentrations normalized by the local mean concentration $C/\overline{C}$, where C is the total (mean plus fluctuating) local instantaneous concentration and $\overline{C}$ is the local mean. This approach quantifies the contributions of instantaneous concentrations above and below the local mean.

Figure 19 shows scalar pdf's at four distances from the bed at a downstream location ($x = 108$ cm) for the $U_\infty = 10$ cm/s flow case.

The legend lists the dimensional distances from the bed, as well as the corresponding distances in viscous wall units. The vertical dotted line indicates $C/\overline{C} = 1$, where instantaneous concentrations equal the mean. Far from the bed (e.g., $z = 40$ mm), there exist a wide range of concentrations relative to the mean, with the most common concentration being zero (or extremely close to zero), and a monotonically decreasing occurance of higher concentrations. This is indicative of a highly filamentous scalar field that has been stirred but not well mixed. Close to the bed (e.g., $z = 1$ mm, which is at the edge of the VSL), the range of existing concentrations is much narrower, with the most likely concentration being $\overline{C}$. This is indicative of a scalar field that has been mixed by the high shear of the VSL, and persists spatially due to low-turbulence intensities. The intermediate curves in the figure show a smooth progression from the near-bed pdf to the freestream behavior.

Figure 20 shows a similar set of pdf's at the same distance from the source, but for three distances from the plume centerline, at a height of $z = 5$ mm.

The centerline curve ($y = 0$) is the $z = 5$ mm curve from Fig. 19; it has a local maximum near $C/\overline{C} = 1$. The effect of moving away from the plume centerline ($y = 2$ cm, $y = 4$ cm) is similar to the effect of moving away from the bed. Away from the centerline, the most likely concentration is near zero, with a monotonic decay in the pdf. Thus, the "trapped" scalar in the VSL is a feature of the near-centerline plume. The scalar enters the VSL primarily at the plume source. Downstream from there, scalars have difficulty exiting (or entering) the VSL due to the low turbulence levels.

Figure 21 shows two near-bed ($z = 1$ mm) pdf's from an upstream ($x = 37$ cm) and a downstream ($x = 108$ cm) location.

The downstream pdf was also shown in Fig. 19. This figure demonstrates that a certain streamwise distance is required before the pdf develops a maximum at $C/\overline{C} = 1$. Close to the source, the pdf has a monotonic decay, despite the proximity to the bed. It takes time (and hence distance) for the high shear near the bed to smear out the

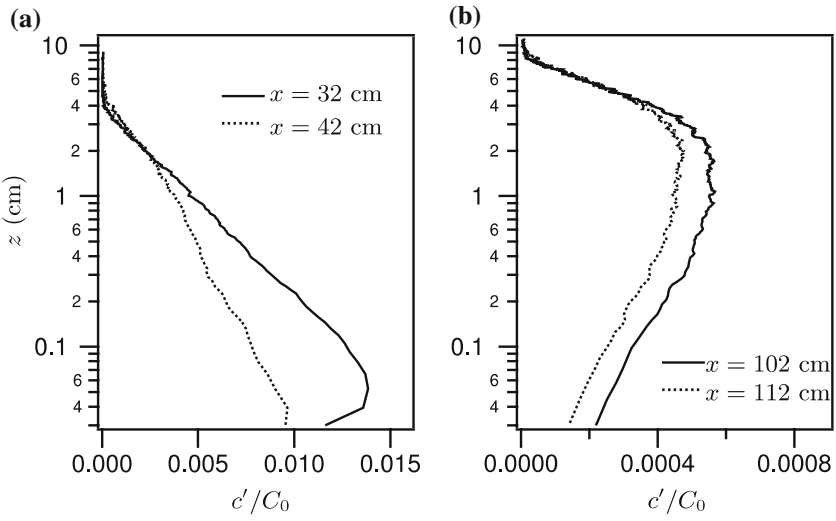

Fig. 17 Vertical profiles (at $y = 0$) of rms concentration fluctuations at two **(a)** upstream and **(b)** downstream streamwsie locations for the $U_\infty = 10$ cm/s flow case

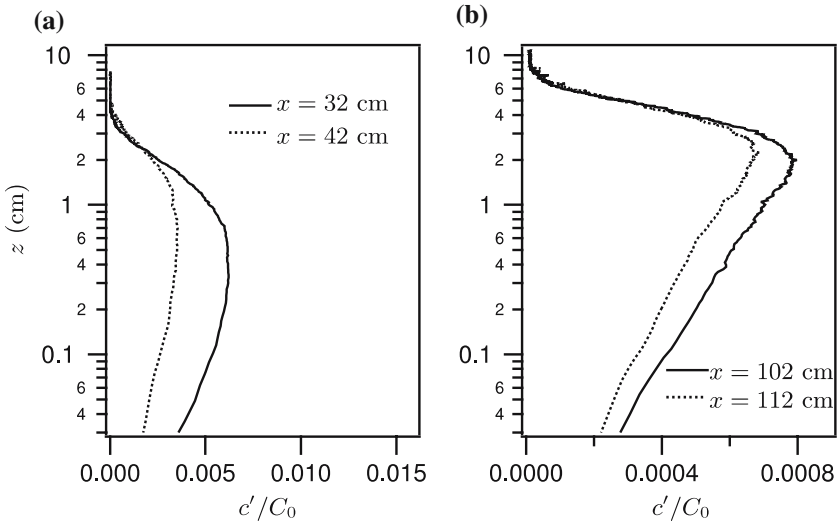

Fig. 18 Vertical profiles (at $y = 0$) of rms concentration fluctuations at two **(a)** upstream and **(b)** downstream streamwsie locations for the $U_\infty = 30$ cm/s flow case. Same scales as Fig. 17

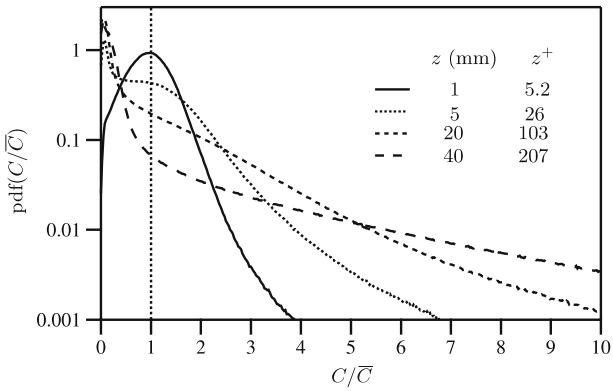

Fig. 19 The pdf's of concentration as a function of height (see legend) at $y = 0$ cm at the downstream location ($x = 108$ cm) for the $U_\infty = 10$ cm/s flow case

concentration fluctuations seen close to the source. The effect is eventually to limit the range of existing concentration values.

5 Discussion and summary

The spatial development of the plume in this study is significantly affected by the interaction of the scalar field with the VSL. This is due to several aspects of the experimental flow. First, the bed is smooth, which permits the formation of the VSL. Second, the Reynolds number of the boundary layer flows is quite low ($Re_\theta = 540$ for the slow case), which results in a thick VSL (approximately 1 mm) relative to the resolution of the PLIF technique (150 μm). Finally, the source is flush with the bed, and

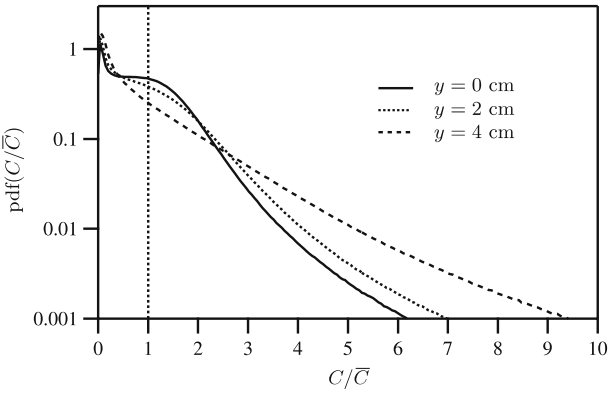

Fig. 20 The pdf's of concentration as a function of distance from the plume centerline (see legend) at $z = 5$ mm at the downstream location ($x = 108$ cm) for the $U_\infty = 10$ cm/s flow case

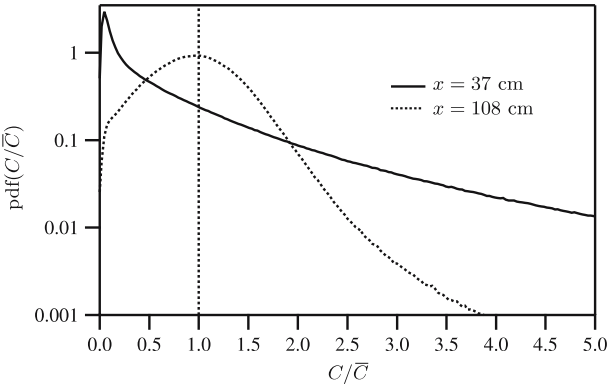

Fig. 21 The pdf's of concentration as a function of distance from the source at $z = 1$ mm on the plume centerline for the $U_\infty = 10$ cm/s flow case

the scalar release is essentially momentumless. The result is that the scalar is infused directly into the VSL, where it has a propensity to persist due to the minimal near-bed stirring. The ability of the scalar to exit the VSL is controlled by a combination of molecular diffusion and turbulent incursions into the layer from above. In previous plume studies, the effect of the VSL was minimized through some combination of bed roughness, Reynolds number, and size, location, and momentum of the source.

We use an idealized analytical plume solutions as a baseline for many comparisons with experimental data. The idealized solution assumes that the flow is shear-free and homogeneous. Because these assumptions are most strongly violated near the bed (and, in particular, in the VSL), it is not surprising that the near-bed behavior of the measured plume deviates most significantly from the idealized solution. The observed deviations are therefore signatures of the shear an inhomogeneity in the flow. The effect of the low mixing rates in the VSL is to "trap" scalar mass that has been released there, and the effect of the shear is to rapidly smear out any scalar fluctuations that are present. These two effects, seemingly at odds with one another, result in the complex observed mean, and fluctuating concentration profiles.

Despite the unique configuration of this study, many of the plume characteristics are in agreement with those reported in previous studies. For example, the lateral mean concentration profiles are Gaussian, with a variance that grows linearly with x, consistent with studies such as (2,5–7). The lateral diffusivities deduced from the measured plume spread are consistent with previously reported values (13). The lateral concentration fluctuation profiles are seen to be either Gaussian or bimodal, consistent with the results and discussion given by Rahman and webster (5).

Not surprisingly, the effect of the VSL manifests itself most significantly in the vertical concentration profiles. While the existence of non-Gaussian profiles is well known (2,5–8), the behavior seen in our study differs. Most studies have reported exponential vertical mean profiles. Some studies report constant values of the exponent α (e.g., 1.4 (2), 1.5 (7)), while others suggest that α decreases slowly with x (8,9,14). Our results show a different behavior, with a small α (corresponding to a strongly non-Gaussian profile) near the source, asymptoting toward $\alpha = 2$ (Gaussian) in the far-field. The small value of α near the source corresponds to a profile with exceptionally high concentrations in the VSL, and very low concentrations above it. This profile is a result of the combined effects of high shear and low mixing in the VSL. As distance from the source increases, the scalar is able to enter the flow above the VSL, and the profile tends toward a Gaussian. Our data suggests that α is a function of x^+. This scaling is consistent with the fact that the viscous unit u_τ/ν is a measure of the thickness of the VSL, and thus x^+ is a measure of the downstream distance relative to the height of the VSL.

The measurements and analysis presented in this paper are likely somewhat unique to flows where a VSL is present. As discussed, prior results (where a VSL was not present) are not in agreement with many results presented herein. Flows with significant roughness, large Reynolds numbers, and source geometries that do not initially confine the scalar to the near-bed region are likely to differ from our results.

Acknowledgements This work was supported by the Office of Naval Research's Chemical Plume Tracing Program, under Grants N00014-00-1-0794 (to JPC), and N00014-97-1-0706, N00014-98-1-0785 (to JRK).

References

1. Crimaldi JP, Koseff JR (2001) High-resolution measurements of the spatial and temporal structure of a turbulent plume. Exp Fluids 31:90–102
2. Bara BM, Wilson DJ, Zelt BW (1992) Concentration fluctutation profiles from a water channel simulation of a ground-level release. Atmos Environ 26A:1053–1062
3. Yee E, Wilson DJ, Zelt BW (1993) Probability-distributions of concentration fluctuations of a weakly diffusive passive plume in a turbulent boundary-layer. Bound-Lay Meteorol 64(4):321–354
4. Webster DR, Rahman S, Dasi LP (2003) Laser-induced fluorescence measurements of a turbulent plume. J Eng Mech ASCE 129(10):1130–1137
5. Rahman S, Webster DR (2005) The effect of bed roughness on scalar fluctuations in turbulent boundary layers. Exp Fluids 38(3):372–384
6. Robins AG (1978) Plume dispersion from ground level sources in simulated atmospheric boundary layers. Atmos Environ 12:1033–1044
7. Fackrell JE, Robins AG (1982) Concentration fluctuations and fluxes in plumes from point sources in a turbulent boundary layer. J Fluid Mech 117:1–26
8. Brown MJ, Arya SP, Snyder WH (1993) Vertical dispersion from surface and elevated releases-an investigation of a non-gaussian plume model. J Appl Meteorol 32(3):490–505
9. Gryning SE, Vanulden AP, Larsen SE (1983) Dispersion from a continuous ground-level source investigated by a k-model. Q J R Meteorol Soc 109(460):355–364

10. Crimaldi JP, Wiley MB, Koseff JR (2002) The relationship between mean and instantaneous structure in turbulent passive scalar plumes. J Turbul 3:1–24
11. Barrett TK (1989) Nonintrusive optical measurements of turbulence and mixing in a stably-stratified fluid. PhD thesis, University of California, San Diego
12. Spalart PR (1988) Direct simulation of a turbulent boundary layer up to $\mathrm{Re}_{\delta_2} = 1410$. J Fluid Mech 187:61–98
13. Fischer HE, List EJ, Koh RC, Imberger J, Brooks NH (1979) Mixing in Inland and coastal waters. Academic Press, Inc., San Diego
14. Hunt JCR, Weber AH (1979) Lagrangian statistical-analysis of diffusion from a ground-level source in a turbulent boundary-layer. Q J R Meteorol Soc 105(444):423–443